BIOCHEMISTRY
including biophysical chemistry & molecular biology
Article

Biochemistry **2009,** *48,* 9221–9233 9221
DOI: 10.1021/bi900935q

The *Escherichia coli* ClpA Molecular Chaperone Self-Assembles into Tetramers†

P. Keith Veronese, Ryan P. Stafford, and Aaron L. Lucius*

Department of Chemistry, The University of Alabama at Birmingham, 1530 3rd. Ave S, Birmingham, Alabama 35294-1240

Received June 3, 2009; Revised Manuscript Received July 30, 2009

ABSTRACT: The *Escherichia coli* ATP-dependent protease, ClpAP, is composed of the hexameric ATPase/protein-unfoldase, ClpA, and the tetradecameric proteolytic component, ClpP. ClpP proteolytically degrades folded proteins only when associated with the motor protein ClpA or ClpX, both of which use ATP binding and/or hydrolysis to unfold and translocate proteins into the tetradecameric serine protease ClpP. In addition to ClpA's role in regulating the proteolytic activity of ClpP, ClpA catalyzes protein unfolding of proteins that display target sequences to "remodel" them, in vivo, for regulatory roles beyond proteolytic degradation. In order for ClpA to bind protein substrates targeted for removal or remodeling, ClpA first requires nucleoside triphosphate binding to assemble into an oligomeric form with protein substrate binding activity. In addition to this nucleotide driven assembly activity, ClpA self-associates in the absence of nucleoside triphosphate binding. An examination of the energetics of the nucleotide driven assembly process cannot be performed without a thermodynamic model of the self-assembly process in the absence of nucleotide cofactor. Here we report an examination of the self-association properties of the *E. coli* ClpA protein unfoldase through the application of analytical ultracentrifugation and light scattering techniques, including sedimentation velocity, sedimentation equilibrium, and dynamic light scattering approaches. In contrast to published results, application of these approaches reveals that ClpA exists in a monomer−tetramer equilibrium (300 mM NaCl, 10 mM $MgCl_2$, and 25 mM HEPES, pH 7.5 at 25 °C). The implications of these results for the *E. coli* ClpA self-association and ligand linked association activities are discussed.

ATP-dependent proteases, in both eukaryotes and prokaryotes, are essential for the removal of damaged or misfolded proteins that can occur during heat shock or stress and are therefore critical components of protein quality control pathways (*1*−*3*). Examples of such ATP-dependent proteases are responsible for the removal of properly folded proteins for cell cycle regulation and homeostasis in all organisms (*4*). *Escherichia coli* ClpAP, like many other energy-dependent proteases, is composed of two distinct enzymes, a protein unfoldase, ClpA, and a protease, ClpP (*5*, *6*). ClpA appears to couple ATP binding and hydrolysis to enzyme-catalyzed protein unfolding and polypeptide translocation, and ClpP accepts and proteolytically degrades the newly unfolded protein (*7*). Similar to ClpAP, the 26 S proteasome, which is the eukaryotic ATP-dependent protease, is also composed of two distinct enzymes. These are a proteolytic component, the 20 S core, and a protein unfoldase, the 19 S cap. Comparable to the bacterial ClpA, the 19 S cap uses its protein unfolding activity to unfold and translocate ubiqutinated proteins. Analogous to the bacterial ClpP, the 20 S core accepts the unfolded protein and catalyzes proteolytic degradation of the substrate (*8*, *9*).

E. coli contains five known ATP-dependent proteases, ClpAP, ClpXP, HslUV (ClpYQ), Lon, and FtsH. In the case of Lon and FtsH, a single transcript contains both the proteolytic and protein unfoldase components (*10*, *11*). In contrast, ClpAP, ClpXP, and HslUV (ClpYQ) are composed of the protein unfoldase component ClpA, ClpX, or HslU (ClpY), respectively, and the proteolytic component ClpP or HslV (ClpQ), respectively (*2*).

The protein unfoldases, ClpA, ClpX, HslU, and the 19 S cap, from sequence analysis, all belong to the ATPases Associated with various cellular Activities (AAA+) family of proteins (*12*). AAA+ proteins are a large superfamily of proteins that include a number of molecular chaperones, some DNA helicases, and cellular cargo transporters such as Dynein (*13*). These AAA+ proteins are defined by a number of conserved regions including the canonical Walker A and Walker B motifs that make up the ATP binding and hydrolysis site, often termed an AAA cassette (*14*).

Strikingly, the ClpA protein contains two of the AAA cassettes per monomer, and therefore contains two ATP binding and hydrolysis sites per monomer (*15*). Current data suggest that ClpA requires nucleoside triphosphate binding but not hydrolysis to assemble into the hexameric form that can associate with ClpP, and thus form an active ATP-dependent protease (*16*). In addition, data suggest that one of the nucleotide binding sites is required for nucleotide driven assembly, whereas the other is required for polypeptide translocation (*17*).

ClpA has been examined with both X-ray crystallography and electron microscopy. Electron microscopy studies show that ClpA forms ring-shaped structures with 6-fold symmetry in the presence of the slowly hydrolyzable nucleotide analogue, ATPγS (*18*).[1] Additionally, sedimentation equilibrium experiments

†P.K.V. was supported by an Alabama EPSCoR Graduate Research Fellowship (GRSP). This work was partially supported by NSF Grant MCB-0843746 to A.L.L. and the University of Alabama at Birmingham Department of Chemistry Start-up Funds.

*To whom correspondence should be addressed. Phone: 205-934-8096; fax: 205-934-2543; e-mail: allucius@uab.edu.

[1]Abbreviations: ATPγS, adenosine 5′-[gamma-thio]-triphosphate; EDTA, ethylenediaminetetraacetic acid disodium salt; NLLS, nonlinear-least-squares.

performed at 4 °C in the presence of ATPγS suggest ClpA forms a hexameric species in solution (*19*). Interestingly, X-ray crystallographic studies with ClpA bound by ADP revealed that ClpA crystallized as a hexameric spiral and not the expected hexameric rings (*20*). Combining the crystal structure with evidence from electron microscopy studies, three-dimensional models of the expected hexameric rings have been reconstructed (*21*).

ClpA requires nucleoside triphosphate binding to assemble into an oligomeric form that will bind to target sequences in protein substrates (*22*). Despite this, the relative affinities for nucleotide binding to each of the two nucleotide binding sites in ClpA are not known. To quantitatively examine the energetics of nucleotide binding, nucleotide driven hexamer formation, and subsequent protein substrate recognition, a thermodynamic model for self-association of ClpA in the absence of nucleotide binding is required. Moreover, the model for self-association of ClpA must be determined under identical conditions (i.e., temperature, salt concentration and type, pH, etc.) as the model for nucleotide driven self-association.

Previous studies have reported that ClpA resides in a mixture of monomers and dimers in the absence of nucleoside triphosphate based on a sedimentation−equilibrium experiment performed at 4 °C (*19*). More recently, Kress and co-workers concluded that ClpA forms transient tetramers in the presence of ATPγS and in the absence of Mg^{2+} at 25 °C using gel-filtration chromatography and stopped-flow static light scattering measurements (*23*). They propose a model for nucleotide driven assembly that assumes ClpA is in a monomer−dimer equilibrium at 25 °C based on previous measurements performed at 4 °C. As such, they conclude that the tetrameric state formed upon addition of nucleotide is a transient intermediate on the pathway to hexamer formation from dimers.

Here we report the results of an examination of the self-association properties of ClpA using analytical ultracentrifugation approaches including sedimentation velocity and sedimentation equilibrium at 25 °C. Our results show that ClpA exists as a mixture of monomers and tetramers at 25 °C at thermodynamic equilibrium. Because of the presence of tetramers at thermodynamic equilbirum, the tetrameric state is not simply a transient intermediate on the pathway to hexamer formation, as previously concluded (*23*). Further, we have confirmed this observation, in a model-independent fashion, by combining sedimentation coefficients acquired from sedimentation velocity experiments with direct measurements of the diffusion coefficient acquired from dynamic light scattering experiments. Finally, we have no evidence for a significantly populated dimeric intermediate at thermodynamic equilibrium at 25 °C.

MATERIALS AND METHODS

Buffers. Buffers were prepared with reagent grade chemicals using twice distilled H_2O. Twice distilled water was produced using the Purelab Ultra Genetic system (Siemens Water Technology). Buffer B is 25 mM Tris, 0.1 mM EDTA, 2 mM 2-mercaptoethanol, 10% glycerol, pH 8.0 at 4 °C and the NaCl concentration is indicated in the text. Buffer H is 25 mM HEPES pH 7.5 at the indicated temperature, 300 mM NaCl, and the $MgCl_2$ concentrations are indicated in the text. Experiments were performed with and without EDTA and no significant differences were observed.

ClpA Protein. We isolated the gene encoding for *E. coli* ClpA directly from the *E. coli* K12 strain. The gene was cloned into the pET30a vector (Novagen). The gene encoding for ClpA was sequenced and found to be identical to the published sequence (Genbank accession number M31045). ClpA was overexpressed from the pET30a vector in BL21(DE3) cells and 100 g of frozen cell paste was suspended in 400 mL of buffer containing 2 mM 2-mercaptoethanol, 10 mM EDTA, 40 mM Tris (pH 8.0), 40 mM spermidine, 200 mM NaCl, 440.6 mM ammonium sulfate, 10% (w/v) sucrose, and 0.2 mM PMSF. Cells were then passed through an ice chilled French press. The nucleic acid was precipitated with 0.3% (v/v) PEI. The resulting supernatant was precipitated with 40% saturation ammonium sulfate. The ammonium sulfate pellet was dissolved in buffer B supplemented with 50 mM NaCl and dialyzed overnight against the same buffer. The sample was loaded onto a Q-Sepharose 6 FF (GE Healthcare) equilibrated with buffer B supplemented with 50 mM NaCl. The sample was eluted with a linear gradient from 50 mM NaCl up to 400 mM NaCl. The fractions containing ClpA were dialyzed overnight against buffer B supplemented with 200 mM NaCl. The sample was loaded onto a Heparin sepharose FF (GE Healthcare) column equilibrated with buffer B supplemented with 200 mM NaCl. The protein was eluted with a linear gradient from 200 mM NaCl to 1 M NaCl. The fractions containing ClpA dialyzed overnight against buffer B supplemented with 200 mM NaCl. The sample was loaded onto Blue Sepharose FF (GE Healthcare) that was equilibrated in buffer B supplemented with 200 mM NaCl. The column was eluted with a linear gradient from 200 mM NaCl to 2 M NaCl. The peak containing ClpA was dialyzed against buffer B supplemented with 1 M NaCl and 50% glycerol for storage at −80 °C. The resultant protein was >95% pure as judged by Coomassie staining. From 100 g of frozen cell paste 800 mg of >95% pure ClpA monomer was acquired using this protocol.

ClpA concentration was determined spectrophotometrically using an extinction coefficient of $(3.1 \pm 0.2) \times 10^4\ M^{-1}\ cm^{-1}$ for the monomer in buffer B. All protein concentrations reported refer to the monomer concentration. This extinction coefficient was determined from comparison of the absorption spectra of several aliquots of denatured ClpA protein in buffer B plus 6 M guanidine-HCl with the absorption spectra of aliquots of native ClpA in buffer B. The extinction coefficient for ClpA in 6 M guanidine-HCl was calculated from the extinction coefficients of the individual aromatic amino acids (3 Trp, 11 Tyr, 27 Phe) in 6 M guanidine-HCl as described (*24*).

Analytical Ultracentrifugation. Analytical ultracentrifugation experiments, both sedimentation velocity and sedimentation equilibrium, were performed using a Beckman Optima XL-A analytical ultracentrifuge. Sedimentation velocity experiments were performed by loading a sample of protein (380 μL) into a double sector Epon charcoal-filled centerpiece and subjected to an angular velocity of 40 000 rpm. Absorbance scans as a function of radial position were collected by scanning the sample cells at a wavelength of 280 nm at intervals of 0.01 cm. Scans were collected every 4 min.

Sedimentation equilibrium experiments were performed by loading a sample of protein (110 μL) into a double sector Epon charcoal-filled centerpiece. Samples were sedimented at the velocity indicated in the text until sedimentation equilibrium was achieved as judged by WinMatch (David Yphantis, University of Connecticut, Jeff Larry, National Analytical Ultracentrifugation Center, Storrs, CT).

Analysis of Sedimentation Velocity Data. Sedimentation velocity boundaries were analyzed using SedFit (Peter Schuck,

NIH), where SedFit generates a c(s) distribution of Lamm equation solutions (*25*). Sedimentation velocity boundaries were also analyzed using Sedfit to generate normalized ls-g*(s) distributions (*26*). The sedimentation coefficient, s, is given by Svedberg's equation, eq 1,

$$s = \frac{M(1-\bar{v}\rho)}{Nf} = \frac{MD(1-\bar{v}\rho)}{RT} \quad (1)$$

where M is the molecular weight, $\bar{v}$, is the partial specific volume of the macromolecule, ρ is the density of the buffer, N is Avogadro's number, f is the frictional coefficient, D is the diffusion coefficient, R is the ideal gas constant, and T is absolute temperature. The two forms of eq 1 are related by eq 2,

$$D = \frac{k_b T}{f} \quad (2)$$

where k_b is Boltzman's constant. For comparison to previously reported weight average sedimentation coefficients, the weight average sedimentation coefficient was calculated from the c(s) distribution by integrating over the area of the c(s) distribution (*27*, *28*). All sedimentation coefficients reported in the text are corrected to 20 °C and infinite dilution in water, $s_{20,w}$.

Analysis of Sedimentation Equilibrium Data. Sedimentation equilibrium boundaries were subjected to global nonlinear-least-squares (NLLS) fitting using the program HeteroAnalysis (James L. Cole and Jeffrey W. Larry, Storrs, CT) (*29*). Using HeteroAnalysis, absorbance profiles as a function of radial position were fit to a sum of exponentials, where each exponential represents a discrete population of an oligomeric species (n-mer) formed from n monomeric units, eq 3,

$$A_T = \sum_{i=1}^{j} A_{f,ref}^{n_i} L_{n_i 0,\,Abs} e^{(n_i \sigma \xi)} + b \quad (3)$$

where A_T is the total absorbance at radial position r, j is the number of species, n_1 is always one, and n_i is the number of monomers in an oligomer, $A_{f,ref}$ is the absorbance of the monomeric species at the reference radial position, r_0, $\xi = (r^2 - r_0^2)/2$, b is a baseline offset term, and σ is the reduced molecular mass of the monomeric species given by eq 4,

$$\sigma = \frac{M(1-\bar{v}\rho)\omega^2}{RT} \quad (4)$$

where M is the molecular mass of the monomer, $\bar{v}$ is the partial specific volume of the monomer, ρ is the density of the solvent, ω is the angular velocity of the rotor, R is the ideal gas constant, and T is the absolute temperature. The partial specific volume of ClpA was calculated from the primary sequence to be $\bar{v}$ = 0.7403 mL g^{-1} using SEDNTERP (David Hayes, Magdalen College, Tom Laue, University of New Hampshire, and John Philo, Alliance Protein Laboratories). The density of the buffer, ρ = 1.04074 g mL^{-1}, was calculated from the buffer components using SEDNTERP.

In eq 3, $L_{n0,Abs}$ is the equilibrium constant in absorbance units for n monomers associating to form an n-mer, eq 5,

$$L_{n_i 0,\,Abs} = \frac{A_{n_i}}{A_{mon}^{n_i}} \quad (5)$$

where A_n is the absorbance of an n-mer and A_{mon} is the absorbance of the free monomer. The equilibrium constant in concentration units, L_{ni0}, is determined by substituting Beer's Law into eq 5 and rearranging to yield eq 6.

$$L_{n_i 0} = L_{n_i 0,\,Abs} \frac{\varepsilon^{n_i - 1} l^{n_i - 1}}{n_i} \quad (6)$$

The reported root-mean-square-deviation (rmsd) was reported by HeteroAnalysis for each NLLS analysis. We subsequently determined the uncertainty associated with the rmsd for comparison purposes using the following equation, which yields the fractional uncertainty on the rmsd value (*30*),

$$\frac{1}{\sqrt{2(N-1)}}$$

where N is the number of data points used in the fit. The uncertainty on the rmsd value is determined by multiplying by the determined rmsd from a given fit.

Weight average $s_{20,w}$ values as a function of the free ClpA concentration were analyzed using eq 7 (*31*),

$$\bar{s}_{20,w} = \frac{(s_{m,20,w} + 4s_{t,20,w}L_{40}[\mathrm{ClpA}]_{free}^{3})}{(1 + 4L_{40}[\mathrm{ClpA}]_{free}^{3})} \quad (7)$$

where eq 7 relates the weight average $s_{20,w}$ to the free ClpA concentration and $s_{m,w,20}$ represents the monomer sedimentation coefficient, $s_{t,w,20}$ represents the tetramer sedimentation coefficient, and L_{40} is defined above. To relate the free ClpA concentration to the total ClpA concentration the conservation of mass equation was used (eq 8), where $[\mathrm{ClpA}]_t$ is the total ClpA concentration.

$$[\mathrm{ClpA}]_t = [\mathrm{ClpA}]_f + 4L_{40}[\mathrm{ClpA}]_f^4 \quad (8)$$

The weight average sedimentation coefficient as a function of the total ClpA concentration, shown in Figure 3A,B, was subjected to NLLS analysis by implicitly solving eqs 7 and 8. This was accomplished using the implicit fitting routine in Micromath Scientist (Micromath, St. Louis, MO).

Dynamic Light Scattering. Dynamic light scattering experiments were performed using an ALV-5022F with goniometer equipped with an ALV-5000E autocorrelator (ALV, Langen Germany). Experiments were performed by passing 1 mL of protein solution at the indicated concentration through a 0.22 μm Millex GV syringe filter (Millipore) directly into a borosilicate glass cuvette. The cuvette containing the filtered protein sample is placed in the instrument and irradiated with a He−Ne laser emitting at 632.8 nm. Normalized autocorrelation functions of the scattered light were collected at 60°, 90°, and 120° relative to the incident light.

Normalized autocorrelation functions were analyzed using eq 9 (*32*),

$$g_2(\tau) = (g_1(\tau))^2 + c \quad (9)$$

where c is a baseline offset and $g_1(\tau)$ is given by eq 10,

$$g_1(\tau) = \sum_i A_i e^{\Gamma_i \tau} \quad (10)$$

where i is the number of diffusing species, A_i is the amplitude of the ith species, and Γ_i is for the ith species given by eq 11,

$$\Gamma_i = D_i q^2 \quad (11)$$

where D_i is the diffusion coefficient for the ith species and q is the scattering vector given by eq 12,

$$q = \frac{4n_o\pi}{\lambda}\sin\left(\frac{\theta}{2}\right) \quad (12)$$

where n_o is the refractive index of the solution, λ is the wavelength of the laser, and θ is the angle of the detector relative to the incident beam.

At a given concentration of ClpA, normalized autocorrelation functions were collected at 60, 90, and 120°. The set of three angles were globally analyzed using eq 8, with $i = 2$, D_i is a global parameter (the same for each trace) and θ is either 60, 90, or 120°. All diffusion coefficients reported in the text are corrected to 20 °C and infinite dilution in water, that is, $D_{20,w}$. The Z-average diffusion coefficient, $D_{z,20,w}$, as a function of the free ClpA concentration was fit to eq 13 (*33*),

$$D_{z,20,w} = \frac{((M_m)D_{m,20,w} + 4(M_t)D_{t,20,w}L_{40}[\mathrm{ClpA}]_{\mathrm{free}}{}^3)}{((M_m) + 4(M_t)L_{40}[\mathrm{ClpA}]_{\mathrm{free}}{}^3)} \quad (13)$$

where $D_{z,20,w}$ is the Z-average diffusion coefficient, L_{40} is as described above, $D_{m,20,w}$ and $D_{t,20,w}$ are the monomer and tetramer diffusion coefficients, respectively, and M_m and M_t are the monomer and tetramer molecular weights, respectively.

The Z-average diffusion coefficient as a function of total ClpA concentration, shown in Figure 6B, was subjected to NLLS analysis by implicitly solving eqs 13 and 8.

The frictional coefficient ratio, f/f_0, can be calculated from a measured $s_{20,w}$ using eq 14 (*34*−*36*).

$$\frac{f}{f_0} = \left(\frac{M^2(1-\bar{v}\rho)^3}{162\pi^2 S_{20,w}^3\eta^3 N_A^2(\bar{v} + \boldsymbol{\delta}\bar{v}_{H_2O})}\right)^{1/3} \quad (14)$$

The frictional coefficient, f, for ClpA was determined from the measured diffusion coefficient using eq 2. The frictional coefficient ratio, f/f_0, was calculated by dividing the measured frictional coefficient by the frictional coefficient of a hydrated sphere with the same volume, f_0. The equation for f_0 was derived by replacing $s_{20,w}$ in eq 14 with eq 1, in the form containing the frictional coefficient, f, and explicitly solving for f_0, which is given by eq 15,

$$f_o = \left(\frac{162\pi^2\eta^3 M}{N_A}(\bar{v} + \boldsymbol{\delta}\bar{v}_{H_2O})\right)^{1/3} \quad (15)$$

where η is the viscosity of water at 20 °C, M is the molecular weight, N_a is Avogadro's number, $\bar{v}$ is the partial specific volume, $\bar{v}_{H_2O}$ is the partial specific volume of pure water at 20 °C, and δ is the degree of hydration of the macromolecule (grams of water bound per gram of macromolecule). The ratio f/f_0 is the frictional coefficient ratio of the macromolecule to the frictional coefficient of a hydrated sphere of identical volume. The degree of hydration, δ, was estimated using the method of Kuntz (*37*), which for ClpA yields 0.4151 g of water bound per gram of protein. This degree of hydration represents an overestimate as it represents the degree of hydration for an equivalent mixture of amino acids that are completely exposed to solution. Previous studies have compared experimentally determined hydration values for folded proteins to that determined by the Kuntz' method and have shown that only 70% of the degree of hydration calculated using the Kuntz' method is associated with the folded protein (*36*, *38*). As such, we have applied this correction factor in our analysis,

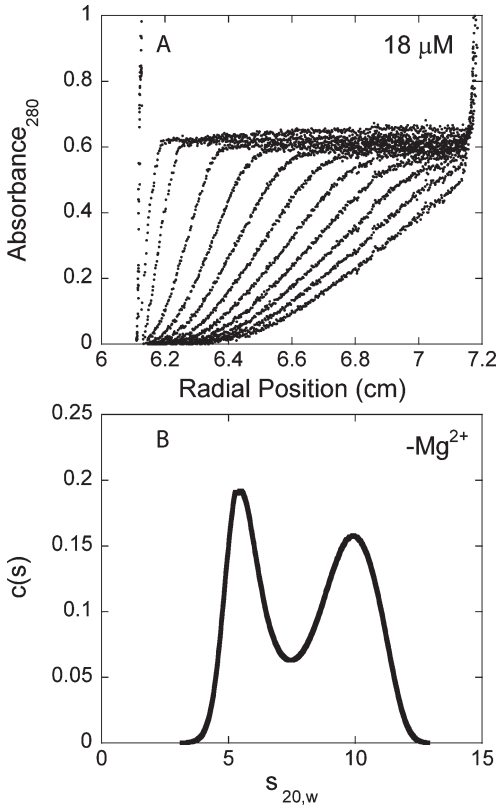

FIGURE 1: Sedimentation velocity experiment of 18 μM ClpA in the absence of Mg^{2+} (A) Representative sedimentation velocity scans collected at 280 nm versus radial position for 18 μM ClpA in buffer H (300 mM NaCl, no Mg^{2+}, 25 °C). For clarity, every fourth scan is shown. (B) c(s) versus $s_{20,w}$ plot from the analysis of the sedimentation velocity scans in panel A. The c(s) analysis reveals a reaction boundary at a [ClpA] = 18 μM in buffer H (300 mM NaCl, no Mg^{2+}, 25 °C) with apparent peaks at 5.46 and 9.96 S.

which yields, $\delta = 0.2906$ g of water per gram of protein. f_{deh} is the frictional coefficient of a dehydrated sphere of equivalent mass and is calculated using eq 15 with $\delta = 0$.

RESULTS

Hydrodynamics of ClpA Examined with Sedimentation Velocity. Sedimentation velocity experiments were performed as described in Materials and Methods. Representative absorbance boundaries collected at 280 nm as a function of radial position are shown in Figure 1A for 18 μM ClpA in buffer H (300 mM NaCl, no $MgCl_2$, 25 °C). The resultant c(s) distribution determined using SedFit, (Peter Schuck, NIH) as described in Materials and Methods, is shown in Figure 1B. The c(s) distribution clearly shows a broad distribution of states. Previously published sedimentation velocity data revealed a weight average sedimentation coefficient, $s_{20,w}$, value of 8.7 S from experiments performed at 20 °C for 2−4 mg/mL (24−48 μM monomer) ClpA (50 mM Tris-HCl pH 7.5 at 25 °C, 300 mM KCl, 1 mM EDTA, 1 mM DTT, and 10% (v/v) glycerol) (*19*). By integrating the c(s) distribution we can determine the weight average sedimentation coefficient. In good agreement with the previously published result of 8.7 S, the weight average $s_{20,w}$, from integration of the c(s) distribution presented in Figure 1B, is 8.59 S for 18 μM ClpA, although the solution conditions are not identical (25 °C and 300 mM NaCl used here vs 20 °C and 300 mM KCl reported previously (*19*)).

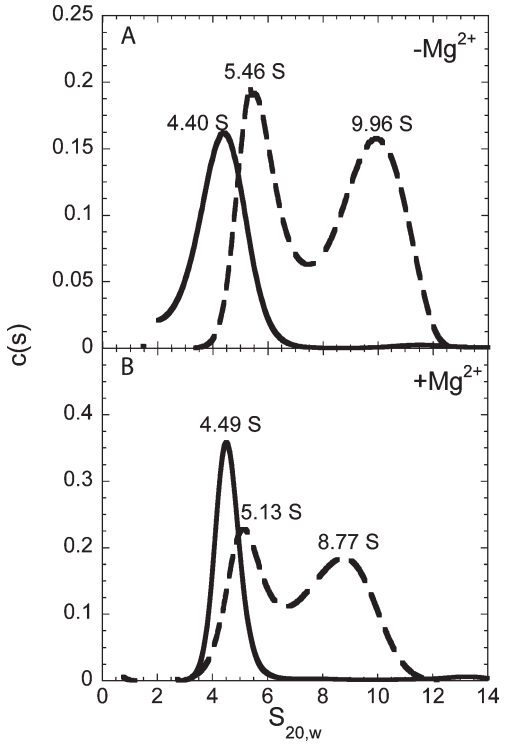

FIGURE 2: Sedimentation coefficient distribution, c(s), dependence on ClpA concentration and Mg^{2+}. c(s) distributions for 1 μM (solid line) and 18 μM (dashed line) ClpA from the analysis of sedimentation velocity experiments performed as described in Materials and Methods in buffer H (300 mM NaCl, 25 °C) both in the (A) absence and in the (B) presence of 10 mM $MgCl_2$. The reaction boundary is labeled according to its apparent peak maximum.

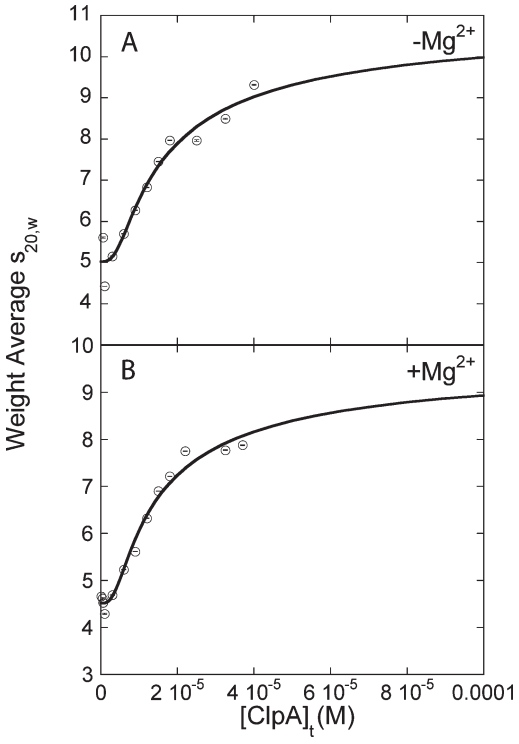

FIGURE 3: Weight average $s_{20,w}$ versus [ClpA]. Plot of weight average $s_{20,w}$ versus [ClpA] for 600 nM to 40 μM ClpA in buffer H (300 mM NaCl, 25 °C) in the (A) absence and (B) presence of 10 mM $MgCl_2$. The solid line is the result of a nonlinear least squares fit to equation 7. The resultant parameters are given in Table 3.

The observed broad distribution in the c(s) plot (Figure 1B) suggests that ClpA self-associates. Because self-association is driven by the free monomer concentration, the shape of the c(s) distribution will depend on ClpA loading concentration, if ClpA is undergoing a self-association reaction. To test this, sedimentation velocity experiments were performed as a function of ClpA loading concentration from 600 nM to 40 μM monomer units. Figure 2A shows the c(s) distribution for 1 μM (solid line) and 18 μM (dashed line) ClpA in buffer H (300 mM NaCl, no $MgCl_2$, 25 °C). Strikingly, at a [ClpA] = 1 μM an apparent single peak with a maximum at 4.40 S is observed and, as the ClpA concentration is increased to 18 μM, the c(s) distribution broadens into a reaction boundary with apparent maxima at 5.46 and 9.96 S, Figures 1B and 2A. Figure 3A shows the weight average $s_{20,w}$ as a function of ClpA loading concentration determined by integrating the c(s) distribution for each sedimentation velocity experiment performed from 600 nM to 40 μM ClpA. Consistent with a self-associating system, the weight average sedimentation coefficient increases with increasing ClpA concentration.

To further illustrate the self-association reaction we have analyzed the sedimentation velocity data using the least-squares g*(s) method, ls-g*(s) (see Materials and Methods). From this analysis, a normalized ls-g*(s) distribution for each loading concentration of ClpA is generated (see Figure 4A). The normalized ls-g*(s) plots clearly shows that at low ClpA concentration (1 μM) an apparent single peak is present. However, as the concentration of ClpA is incrementally increased, the peak broadens into a reaction boundary as expected for a self-associating system that interacts on the time scale of sedimentation (*39*, *40*).

It has been previously established that ClpA requires nucleoside triphosphate and $MgCl_2$ to assemble into an oligomeric form capable of associating with the ClpP protease (*16*). However, the assembly state of ClpA in the absence of nucleotide but in the presence of $MgCl_2$ alone has not been reported. To determine the effect of $MgCl_2$ on the self-association of ClpA, we began by performing a series of sedimentation velocity experiments as a function of [ClpA] from 450 nM to 40 μM in the presence of $MgCl_2$ without nucleoside triphosphate. The c(s) distribution for 1 μM (solid line) and 18 μM (dashed line) [ClpA] are shown in Figure 2B (buffer H, 300 mM NaCl, 10 mM $MgCl_2$, 25 °C). As observed in the absence of Mg^{2+} (Figure 2A), when Mg^{2+} is present at a [ClpA] = 1 μM an apparent single peak is observed with a peak maximum at 4.49 S. Further, as the loading concentration of ClpA is increased, the peak broadens into a reaction boundary with apparent maxima at 5.13 and 8.77 S (Figure 2B). Similar to what was observed in the absence of Mg^{2+}, the weight average sedimentation coefficient increases with increasing ClpA loading concentration when Mg^{2+} is present, see Figure 3B. Therefore, both in the presence and in the absence of Mg^{2+}, the weight average sedimentation coefficient increases with increasing ClpA loading concentration, consistent with a self-associating system. Likewise, the normalized ls-g*(s) distributions, illustrated in Figure 4B, show that the apparent single peak observed at low ClpA concentration broadens with increasing concentration. Thus, in the presence of Mg^{2+} the normalized ls-g*(s) distributions are consistent with a reaction boundary for a self-associating system.

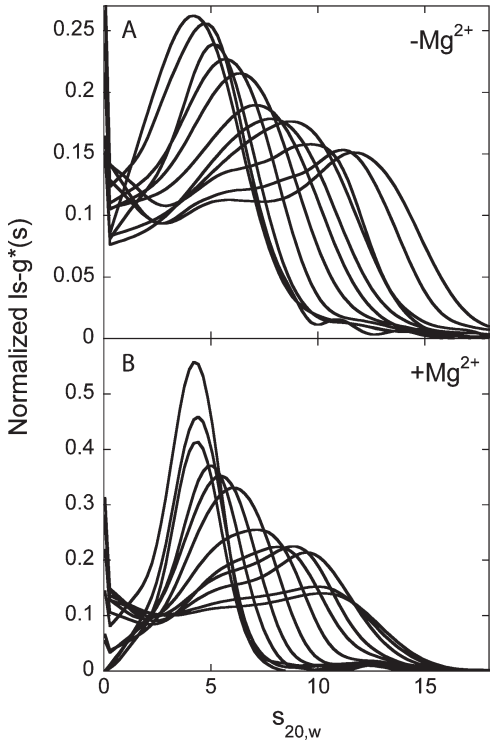

FIGURE 4: Normalized ls-g*(s) distributions. Normalized ls-g*(s) distributions for (A) 600 nM to 40 μM ClpA in the absence of Mg^{2+} and (B) 450 nM to 40 μM ClpA in the presence of Mg^{2+}. In both panels the peak broadens to higher sedimentation coefficient values as the concentration of ClpA is increased.

Examination of the ClpA Assembly State in the Presence of Mg^{2+}. Both the c(s) and ls-g*(s) distributions are consistent with a reaction boundary for a self-associating system. Therefore, from such an analysis, it is difficult to determine the number of species in the distribution. Likewise, because sedimentation coefficients depend on both molecular weight and the frictional coefficient or diffusion coefficient (see eq 1) it is also difficult to determine the molecular weights of each species from sedimentation coefficients alone. Therefore, sedimentation equilibrium experiments were performed to estimate the number of species present, the molecular weights of the species, and the energetics of the self-association reaction in the presence of Mg^{2+}.

Sedimentation equilibrium experiments were performed as described in Materials and Methods at five ClpA loading concentrations and three velocities, Figure 5A−D. The solid lines through the data points are the result of a global nonlinear-least-squares (NLLS) fit of the data to a model containing two species, as given by eq 3 with $j = 2$. Attempts to describe the data with three species ($j = 3$) did not significantly improve the fit (see analysis below). The resulting best fit parameters are $M = (83\,500 \pm 2\,250)$ Da, $n_2 = 4.01 \pm 0.06$, and $L_{40} = (2.40 \pm 0.003) \times 10^{14}$ M^{-3}, with L_{40} obtained in a fit where n_2 is constrained to the nearest integer, 4.0. In this fit a root-mean-square-deviation, rmsd = $(9.23 \pm 0.2) \times 10^{-3}$ (Table 1), was obtained. The molecular weight of the small species, $(83\,500 \pm 2\,250)$ Da, is in good agreement with the ClpA monomer molecular weight, 84 200 Da, calculated from the primary sequence (see Table 1). The molecular weight of the large order species is determined from ($n_2 \times M$), which yields a molecular weight of $(334\,750 \pm 10\,500)$ Da (see Table 1), consistent with a tetramer of ClpA ($4 \times 84\,200$ Da = 336 800 Da). Therefore, in the presence of 10 mM $MgCl_2$ at 25 °C, sedimentation equilibrium experiments performed on ClpA are best described by a monomer−tetramer model.

In further analysis of the sedimentation equilibrium data presented in Figure 5A−D, we performed NLLS analysis of the data to a monomer-*n*-mer model using eq 3 with $j = 2$. In this examination we constrained the monomer molecular weight to 84 200 Da and the large species to $n_2 = 2$, 3, 4, 5, or 6, which corresponds to a dimer, trimer, tetramer, pentamer, or hexamer, respectively. Figure 6A shows a plot of the resultant root-mean-square deviation (rmsd) from each of these NLLS fits. Figure 6A clearly shows that the monomer−tetramer model gives the lowest rmsd and thus the best description of the experimental data.

Examination of the ClpA Assembly State in the Absence of Mg^{2+}. Sedimentation equilibrium experiments were also performed in the absence of Mg^{2+} to estimate the number of species, the molecular weights of the species and the energetic of the self-association reaction. Sedimentation equilibrium experiments were performed at three loading concentrations and three velocities. The resultant absorbance vs radial position plots are shown in Figure 7A−C. The solid lines through the data points are the result of a global NLLS fit of the data to a model containing two species as given by eq 3 with $j = 2$. The resulting best fit parameters are $M = (78\,500 \pm 3\,750)$ Da, $n_2 = 3.94 \pm 0.11$, and $L_{40} = (2.26 \pm 0.003) \times 10^{14}$ M^{-3}, with L_{40} obtained by fitting the data with n_2 constrained to the nearest integer value, 4.0. The root-mean-square-deviation for this analysis was rmsd = $(1.42 \pm 0.03) \times 10^{-2}$ (see Table 1). Therefore, in the absence of Mg^{2+}, a fit of the experimental data yields a molecular weight in good agreement with the molecular weight for a monomer of ClpA, 84 200 Da, calculated from the primary sequence. The molecular weight of the large order species yields a molecular weight of $(309\,750 \pm 17\,250)$ Da, consistent with a tetramer of ClpA ($4 \times 84\,200$ Da = 336 800 Da). As such, from the NLLS analysis, the sedimentation equilibrium data are best described by a monomer−tetramer model both in the presence and absence of 10 mM $MgCl_2$ at 25 °C.

Similar to the analysis of the sedimentation equilibrium experiments in the presence of Mg^{2+}, we reanalyzed the sedimentation equilibrium experiments collected in the absence of Mg^{2+} to a monomer-*n*-mer model, eq 3 with $j = 2$. In this analysis, we constrained the monomer molecular weight to 84 200 Da and constrained $n_2 = 2$, 3, 4, 5, or 6. The resultant rmsd values as a function of n_2 are plotted in Figure 6B. Similar to the sedimentation equilibrium experiments performed in the presence of Mg^{2+}, in the absence of Mg^{2+} the NLLS fit clearly has the lowest rmsd at $n = 4$. Thus, the data are best described by a monomer−tetramer model.

Previous studies concluding that ClpA exists in a monomer−dimer equilibrium in the absence of nucleotide cofactor were performed in the presence of 300 mM KCl as opposed to the 300 mM NaCl we report using here. To test the possibility that KCl may be the reason for the observed difference, sedimentation equilibrium experiments were performed by replacing the 300 mM NaCl with 300 mM KCl (data not shown). The results of the global NLLS are best described by a monomer−tetramer model with similar parameters as determined in the presence of 300 mM NaCl (data not shown).

Modeling of Sedimentation Equilibrium Data in the presence and Absence of Mg^{2+}. Sedimentation equilibrium experiments performed on ClpA in both the presence and absence of Mg^{2+} are best described by a two species model. Moreover,

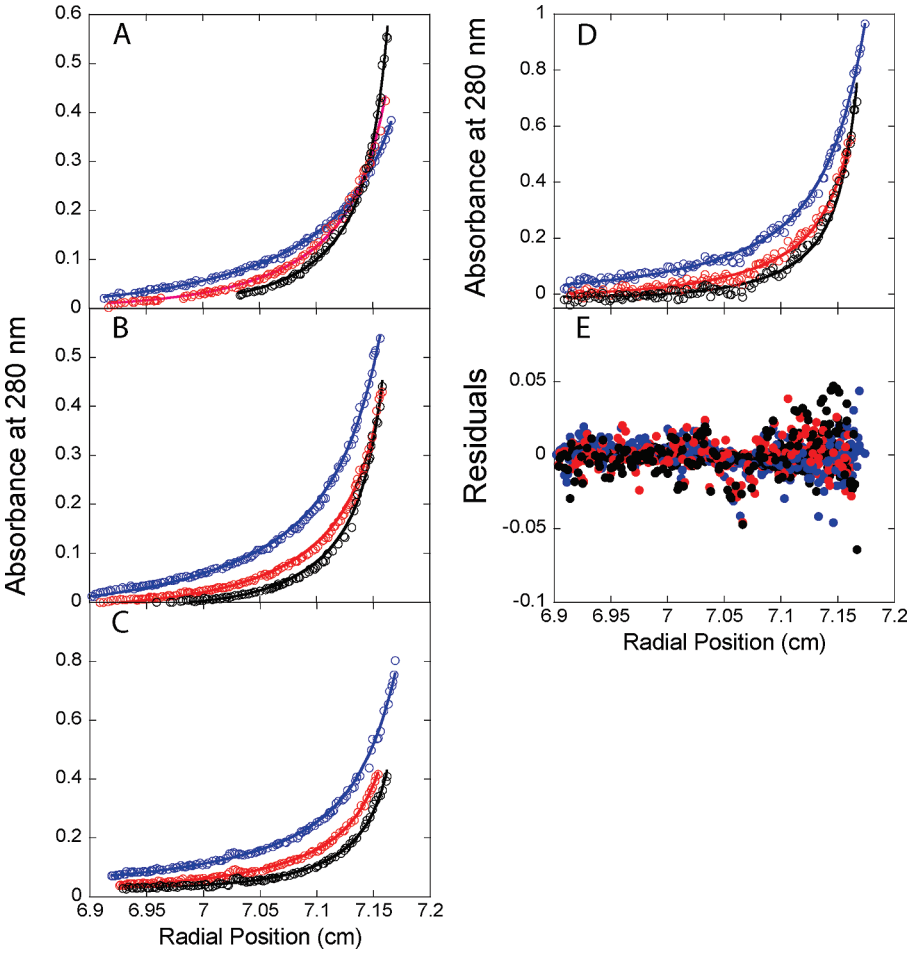

FIGURE 5: Global fitting of sedimentation equilibrium data at 25 °C. (A−D) Result of global fitting of sedimentation equilibrium scans of 4, 6, 9, and 18 μM ClpA in buffer H (300 mM NaCl, 25 °C) with 10 mM $MgCl_2$ at 12 (blue), 15 (red), 18 000 (black) rpm using HeteroAnalysis (James L. Cole and Jeffrey W. Larry, Storrs, CT). Absorbance scans were taken at 280 nm. Open circles represent experimental data points while solid lines represent the result of the global fit. (E) Plot of residuals resulting from global fit.

Table 1: Results of Analysis of Sedimentation Equilibrium Data

buffer H	monomer MW (Da)	n_2	oligomer MW (Da)	L_{40} (M^{-3})[a]	rmsd
$+Mg^{2+}$	83 500 ± 2 250	4.01 ± 0.06	334 750 ± 10 500	(2.40 ± 0.003) × 10^{14}	(9.23 ± 0.2) × 10^{-3}
$-Mg^{2+}$	78 500 ± 3 750	3.94 ± 0.11	309 750 ± 17 250	(2.26 ± 0.003) × 10^{14}	(1.42 ± 0.03) × 10^{-2}

[a] L_{40} determined from constraining n = 4.0.

in both cases, the best fit suggests that ClpA is in a monomer−tetramer equilibrium. However, the NLLS fitting alone does not rule out the possibility of the existence of trimers and hexamers populated such that an apparent tetramer is observed. Additionally, it does not rule out the possibility that a dimeric intermediate could exist, but is not significantly populated.

To examine these possibilities we have subjected the sedimentation equilibrium data collected in the presence and absence of Mg^{2+} (see Figures 5 and 7, respectively) to NLLS analysis to several different possible models and compared the root-mean-squared-deviation of each fit. First, we analyzed the data using a monomer−trimer−hexamer model (eq 3, with three species). In this examination, we subjected the data to NLLS analysis using eq 3 with $j = 3$, $n_1 = 1$, $n_2 = 3$, and $n_3 = 6$. Further, we constrained the monomer molecular weight to 84 200 Da, and allowed L_{30} (monomer to trimer equilibrium constants) and L_{60} (monomer to hexamer equilibriurm constant) to float. Both in the presence and absence of Mg^{2+}, L_{30} tends to float to zero or a small value, that is, $< 1 \times 10^{-15}$. When L_{30} floats to zero or a very small value, eq 3 collapses to a model with $j = 2$; thus, this result suggests that there is not sufficient information in the data for a third species. The rmsd values from the NLLS analysis using a monomer−trimer−hexamer model for the data collected in the presence and absence of Mg^{2+} are (1.143 ± 0.02) × 10^{-2} and (1.693 ± 0.04) × 10^{-2}, respectively. In both cases, these rmsd values are larger than the values determined when subjecting the data to a NLLS fit to a monomer−tetramer model, that is, (9.23 ± 0.2) × 10^{-3} and (1.42 ± 0.03) × 10^{-2} with and without Mg^{2+}, respectively (see Table 1). In addition, we have forced the trimer equilibrium constant, L_{30}, to have various finite values and allowed the hexameric equilibrium constant, L_{60}, to float accordingly. In all cases the rmsd is never lower than the rmsd determined when fitting to a monomer−tetramer model. Therefore, the data are

clearly better described by a monomer−tetramer model than a monomer−trimer−hexamer model.

One additional possibility is that ClpA resides in a monomer−dimer−tetramer equilibrium, but the dimeric intermediate is not significantly populated and thus we only observe monomers and tetramers, that is to say, cooperative association of dimers to form tetramers. To test this possibility, we subjected the sedimentation equilibrium data to NLLS analysis using eq 3 with $j = 3$, $n_1 = 1$, $n_2 = 2$, and $n_3 = 4$, a monomer−dimer−tetramer model. Here, we constrained the monomer molecular weight to 84 200 Da, and allowed L_{20} and L_{40} to float; see Table 2 for the results of the analysis of sedimentation equilibrium data with and without Mg^{2+}. Similar to the analysis with a monomer−trimer−hexamer model, here, the dimerization equilibrium constant, L_{20}, tends to float to zero or a very small value, consistent with the hypothesis that there is little information in the data for a third species. We also performed this analysis by constraining the dimerization equilibiurm constant, L_{20}, to finite values ranging from 1×10^2 to 1×10^5 M^{-1}, but did not see significant improvement in the rmsd; see Table 2 for with and without Mg^{2+}. In fact, at 1×10^5 M^{-1} and above the rmsd value begins to increase, indicated a worse fit. In summary, the data are best described by a monomer−tetramer equilibrium. However, because the rmsd values are not significantly different for L_{20} between zero and 1×10^4 M^{-1}, we cannot rule out the possibility of a dimeric state that is not significantly populated under these conditions, $L_{20} < 1 \times 10^4$ M^{-1}, see Discussion.

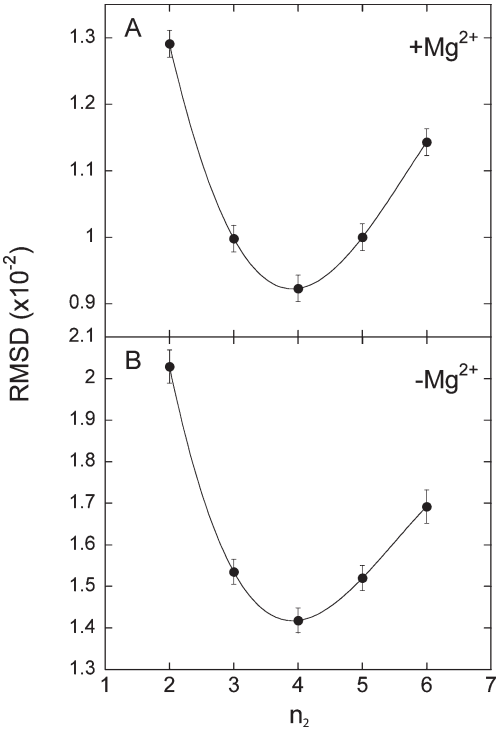

FIGURE 6: rmsd as a function of oligomer size. rmsd as a function of integer oligomer sizes in the (A) presence and (B) absence of Mg^{2+}. Note the minimum in both plots is at a value of $n_2 = 4$, indicating that the best description of the experimental data is to a monomer−tetramer model.

Modeling of the Weight Average $s_{20,w}$ as a Function of ClpA Loading Concentration. The examination of the sedimentation equilibrium experiments, presented above, clearly show that the self-association reaction for ClpA can be best described by a monomer−tetramer equilibrium, both in the presence and absence of Mg^{2+}. If true, the dependence of the weight average sedimentation coefficient, presented in Figure 3, on ClpA loading concentration can be described by the same monomer−tetramer model.

With the above in mind, the weight average sedimentation coefficient as a function of the total ClpA concentration, shown in Figure 3A,B, both in the absence and presence of Mg^{2+}, respectively, were subjected to NLLS fitting using eq 7. Equation 7 describes the dependence of the weight average sedimentation coefficient on the free ClpA monomer concentration (see Materials and Methods). Such an examination yields a measure of the

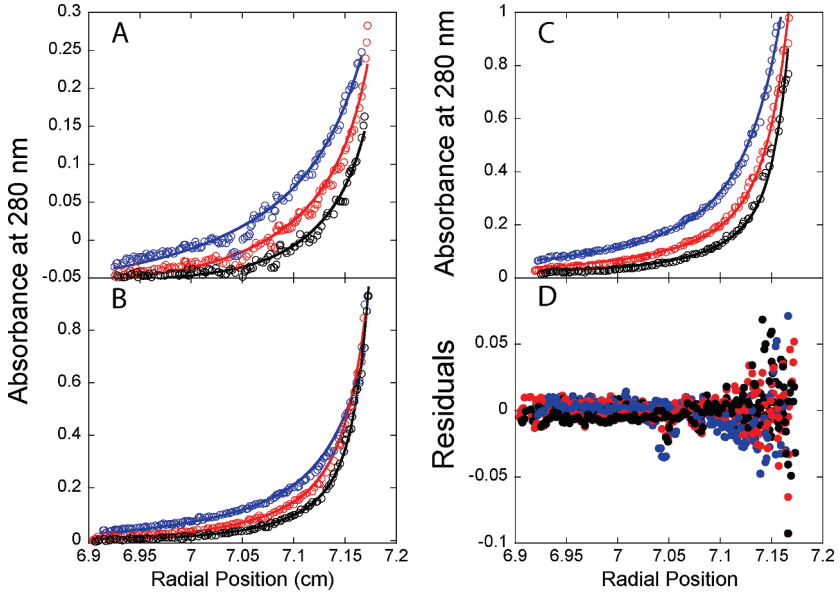

FIGURE 7: Global fitting of ClpA without Mg^{2+} sedimentation equilibrium data at 25 °C. (A−C) Result of global fitting of sedimentation equilibrium scans of 6, 9, and 18 μM ClpA in buffer H (300 mM NaCl, 25 °C) at 12 (blue), 15 (red), 18 000 (black) rpm using HeteroAnalysis (James L. Cole and Jeffrey W. Larry, Storrs, CT). Absorbance scans were taken at 280 nm. Open circles represent experimental data points, while solid lines represent the result of the global fit. (D) Plot of residuals resulting from the global fit.

sedimentation coefficient for the monomeric species at low ClpA concentration, a sedimentation coefficient for the tetramer of ClpA extrapolated to infinite ClpA concentration, and an additional estimate of the monomer−tetramer equilibrium constant, L_{40}. Table 3 shows the result of the NLLS analysis of the weight average sedimentation coefficients as a function of the total [ClpA] shown in Figure 3A,B. The monomer−tetramer equilibrium constants, L_{40}, determined from this analysis are in agreement with those determined from the sedimentation equilibrium experiments; compare values in Tables 1−3.

Because a single species is observed at 1 μM ClpA (see Figure 2) both in the presence and absence of $MgCl_2$, the sedimentation coefficient for the monomer is well determined from the plot at low ClpA concentration to be (4.5 ± 0.1) S and (5.0 ± 0.2) S in the presence and absence of Mg^{2+}, respectively (see Table 3). The sedimentation coefficient for the tetramer is determined from the predicted maximum sedimentation values at infinite ClpA concentration to be (9.8 ± 0.3) S and (11.08 ± 0.7) S in the presence and absence of Mg^{2+}, respectively (see Table 3).

Table 2: Results of NLLS Analysis Using a Monomer−Dimer−Tetramer Model for Sedimentation Equilibrium Experiments Collected in the Presence and Absence of Mg^{2+} (Data presented in Figure 5 and 7)

buffer H	L_{20} (M^{-1})	L_{40} (M^{-3})	rmsd
$+Mg^{2+}$	0	2.05×10^{14}	0.00923 ± 0.0002
$+Mg^{2+}$	1×10^{2}	2.19×10^{14}	0.00965 ± 0.0002
$+Mg^{2+}$	1×10^{3}	2.18×10^{14}	0.00922 ± 0.0002
$+Mg^{2+}$	1×10^{4}	2.69×10^{14}	0.00926 ± 0.0002
$+Mg^{2+}$	1×10^{5}	8.24×10^{14}	0.01031 ± 0.0002
$-Mg^{2+}$	0	2.35×10^{14}	0.01419 ± 0.0003
$-Mg^{2+}$	1×10^{2}	2.38×10^{14}	0.01420 ± 0.0003
$-Mg^{2+}$	1×10^{3}	2.44×10^{14}	0.01419 ± 0.0003
$-Mg^{2+}$	1×10^{4}	3.20×10^{14}	0.01423 ± 0.0003
$-Mg^{2+}$	1×10^{5}	1.29×10^{15}	0.01515 ± 0.0003

Table 3: Parameters for NLLS Fitting of Weight Average Sedimentation Coefficient in Figure 3

buffer H	monomer $S_{20,w}$	tetramer $S_{20,w}$	L_{40} (M^{-3})
$+Mg^{2+}$	4.5 ± 0.1	9.80 ± 0.3	$(2.93 \pm 1.0) \times 10^{14}$
$-Mg^{2+}$	5.0 ± 0.2	11.08 ± 0.7	$(1.95 \pm 1.2) \times 10^{14}$

The sedimentation coefficient determined for the tetrameric state was determined from extrapolation to infinite ClpA concentration from the weight average sedimentation coefficient as a function of ClpA concentration (Figure 3A,B). This extrapolation represents our best estimate for the sedimentation coefficient for the ClpA tetramer (see Table 3). Previous studies have shown that the ratio of the sedimentation coefficient for the large species to the sedimentation coefficient of the monomer should fall between 2.00−2.26 for a tetramer (*41*). Moreover, the ratio for a linear tetramer is 2.00, for a square planar tetramer, 2.20, and for a tetrahedral tetramer, 2.26. In our examination this ratio is ~2.2 both in the presence and absence of Mg^{2+}, consistent with a square planar tetramer of ClpA.

Dynamic Light Scattering. Sedimentation velocity experiments suggested that ClpA self-associated and sedimentation equilibrium experiments are consistent with two sedimenting species with molecular weights consistent with a monomer and a tetramer. To further test this model we used dynamic light scattering techniques to determine the diffusion coefficient. The rationale for this experiment is that the molecular weight of the two species can be acquired by dividing the sedimentation coefficient determined from the analysis of the weight average diffusion coefficient presented in Figure 3A,B by a measure of the diffusion coefficient, see eq 1. Unlike sedimentation equilibrium experiments, determining the molecular weight by dividing the measured sedimentation coefficient by the measured diffusion coefficient does not rely entirely on NLLS fitting. Thus, such an approach can serve as further verification of the fitting model used to analyze sedimentation equilibrium experiments.

Dynamic light scattering experiments were performed as described in Materials and Methods. Representative autocorrelation functions collected at 60, 90, and 120° relative to the incident beam are shown in Figure 8A for 18 μM ClpA in buffer H (300 mM NaCl, 10 mM $MgCl_2$, 25 °C). The solid lines are the result of a global NLLS fit of the data to eq 10 with $i = 2$. Normalized autocorrelation functions were collected from 3−18 μM ClpA. From the global NLLS analysis, two diffusion coefficients are determined at each ClpA concentration, see Figure 8B. Independent of the ClpA concentration a species with $D_{20,w} = (8 \pm 1) \times 10^{-8}$ cm^2 s^{-1} is observed (solid squares in Figure 8B). The second

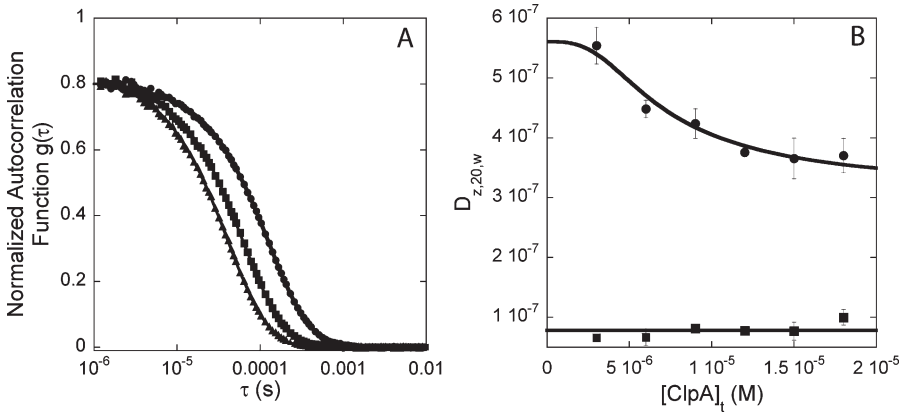

FIGURE 8: Dynamic light scattering. (A) Example of normalized autocorrelation functions for ClpA in buffer H collected at 60 (circles), 90 (squares), and 120° (triangles) solid lines are the result of a global NLLS fit using eq 10 with $i = 2$. (B) Plot of the two Z-average diffusion coefficients from the NLLS analysis in panel A as a function of total [ClpA]. The solid black squares show a diffusion coefficient that is independent of [ClpA] with the solid line representing the average, the solid circles represent the Z-average diffusion coefficient that depends upon [ClpA]. The solid line represents the NLLS fit of the data to eq 13; see Table 3 for parameters.

Table 4: Results from Dynamic Light Scattering Measurements

buffer H	monomer $D_{20,w}$ (10^{-7} cm^2 s^{-1})	tetramer $D_{20,w}$ (10^{-7} cm^2 s^{-1})	monomer MW[a] (Da)	tetramer MW[a] (Da)	ratio[b]
$+Mg^{2+}$	5.6 ± 0.3	2.9 ± 0.3	86 500 ± 5 000	360 000 ± 40 000	4.2 ± 0.5
$-Mg^{2+}$	6.2 ± 0.2	3.2 ± 0.1	87 500 ± 3 000	369 900 ± 15 000	4.2 ± 0.2

[a]Molecular weight calculated based on rearranging eq 1 to $s_{20,w}/D_{20,w}[RT/(1-\bar{v}\rho)]$, values for $s_{20,w}$ are from Table 4, which are predicted from analysis of the weight average sedimentation coefficient as a function of [ClpA] in Figure 3A,B. [b]The ratio is calculated as the molecular weight of the tetramer divided by the molecular weight of the monomer.

diffusion coefficient depends upon ClpA concentration and most likely represents the transition from monomers at low [ClpA] to tetramers at high [ClpA] (solid circles in Figure 8B).

The diffusion coefficient determined in this way has been shown to represent a Z-average diffusion coefficient (*33*). Thus, the dependence of the diffusion coefficient on ClpA concentration was examined using eq 13, which relates the Z-average diffusion coefficient, $D_{z,20,w}$ to the free ClpA concentration. From this analysis it was determined that the monomer $D_{20,w} = (5.6 \pm 0.3) \times 10^{-7}$ cm^2 s^{-1} and the tetramer $D_{20,w} = (2.9 \pm 0.3) \times 10^{-7}$ cm^2 s^{-1} (see Table 4).

Combining the measured sedimentation coefficient of (4.5 ± 0.1) S, reported in Table 3 with the measured diffusion coefficient of (5.6 ± 0.3) × 10^{-7} cm^2 s^{-1} reported in Table 4 a molecular weight of (86 500 ± 5 000) Da was determined, in agreement with a monomer of ClpA (84 200 Da). Likewise, combining the sedimentation coefficient and diffusion coefficient for the larger species, (9.8 ± 0.3) S and (2.9 ± 0.3) × 10^{-7} cm^2 s^{-1}, respectively, a molecular weight of (360 000 ± 40 000) Da is determined, in agreement with a tetramer of ClpA (see Table 4).

The identical approach was taken with ClpA in the absence of Mg^{2+} and the results are given in Table 4. In the absence of Mg^{2+} the data are also consistent with a monomer−tetramer equilibrium.

Hydrodynamic Properties of ClpA. From the measured diffusion coefficient we can calculate the frictional coefficient, f, for both the monomeric state and the tetrameric state of ClpA (see eq 2). Likewise, using eq 15, we can calculate the frictional coefficient for a hydrated sphere of equivalent mass, f_0. The frictional coefficient ratio, f/f_0, can then be determined, where the frictional coefficient ratio is sensitive to the overall shape of each species. The experimentally determined values for the frictional ratio, f/f_0, for the ClpA monomer and tetramer in the presence of Mg^{2+} are 1.18 ± 0.06 and 1.40 ± 0.1, respectively (see Table 5). In the absence of Mg^{2+} the frictional ratios for the monomer and the tetramer are 1.06 ± 0.03 and 1.30 ± 0.04, respectively (see Table 5). Table 5 also includes a calculation of the frictional ratio by comparing the ClpA frictional coefficient to a dehydrated sphere of equivalent mass, f/f_{deh}, (see eq 15 with $\delta = 0$). The frictional coefficient ratios are different when determined by comparing the ClpA frictional coefficient to a dehydrated sphere versus comparison to a hydrated sphere. This difference suggests that ClpA may be significantly hydrated.

Table 5 shows that a significant change in the frictional coefficient is observed for ClpA monomer versus the ClpA tetramer both in the presence and absence of Mg^{2+}. The previously determined X-ray crystal structure of the ClpA monomer shows an elongated structure (*20*). The elongated structure observed in the crystal would be consistent with a prolate ellipsoid with a long axis, $a = 13.03$ nm, and a short axis, $b = 6.37$ nm. From this structure the axial ratio, $a/b = 2.04$. Using our experimentally determined frictional coefficient ratios we can calculate the axial ratio by modeling each species to a prolate ellipsoid. Modeling the ClpA monomer to a prolate ellipsoid results in an axial ratio of 3.90 ± 0.2 and 2.28 ± 0.07 in the presence and absence of Mg^{2+}, respectively (see Table 5). Interestingly, in the absence of Mg^{2+} the experimental axial ratio is similar to that determined from the X-ray crystal structure. In contrast, in the presence of Mg^{2+}, the axial ratio is nearly 2-fold larger relative to the axial ratio for the crystal structure, suggesting a more elongated structure in the presence of Mg^{2+}.

Table 5: Hydrodynamic Properties of ClpA

	buffer H	f/f_{deh}	f/f_0	a/b[a]
monomer	$+Mg^{2+}$	1.31 ± 0.07	1.18 ± 0.06	3.90 ± 0.2
tetramer	$+Mg^{2+}$	1.60 ± 0.10	1.40 ± 0.10	7.96 ± 0.8
monomer	$-Mg^{2+}$	1.19 ± 0.04	1.06 ± 0.03	2.28 ± 0.07
tetramer	$-Mg^{2+}$	1.44 ± 0.05	1.30 ± 0.04	5.73 ± 0.1

[a]Axial ratio, a/b, calculated using a prolate ellipsoid model.

Both in the presence and absence of Mg^{2+} the axial ratio for the tetramer is significantly different from that of the corresponding monomer. These results suggest that upon tetramer formation, a more elongated structure results compared to that of the monomer. Moreover, the tetramer formed in the presence of Mg^{2+} is more elongated than the tetramer formed in the absence, 7.96 ± 0.8 and 5.73 ± 0.1, respectively. These results are consistent with a significant conformational change in the presence of Mg^{2+}.

DISCUSSION

The long-term goal of our research is to correlate the assembly state of ClpA with ATP binding and hydrolysis and protein substrate binding and translocation. To do this, however, we must have knowledge of the assembly state under the same solution conditions where we will examine the enzymatic activities. Previously reported sedimentation velocity experiments were carried out at 20 °C and evidence for two sedimenting species was presented, similar to what we report here (*19*). However, molecular weight determinations of the two species were determined with sedimentation equilibrium experiments performed with two ClpA concentrations (~2.4 and 6 μM monomer) and a single velocity (7000 rpm) at 4 °C, where it was concluded that ClpA exists in a monomer−dimer equilibrium (*19*). In contrast, sedimentation velocity and sedimentation equilibrium experiments, reported here, to examine the self-association properties of ClpA were all performed at 25 °C. Because the self-association equilibrium constants will depend on temperature, it is possible that the monomer−tetramer equilibrium constant is weak at 4 °C and thus only monomers and dimers were previously observed. Therefore, it is possible that as the temperature is increased to 25 °C the monomer−tetramer equilibrium constant is significantly increased and one no longer

observes dimers, but instead observes a monomer−tetramer equilibrium as reported here.

We have performed a series of simulations to illustrate how a monomer−dimer−tetramer equilibrium may persist even when experimentally one only observes monomers and tetramers. We have simulated the species fractions for a monomer−dimer−tetramer equilibrium for various values of the stepwise equilibrium constants L_{20} and L_{40}^{x}, where L_{20} is the equilibrium constant for two monomers forming a dimer (see eqs 16 and 18) and L_{40}^{x} is the equilibrium constants for two dimers forming a tetramer (see eqs 17 and 19) and L_{40} is the overall equilibrium constant for four monomers forming a tetramer as given by eq 20.

$$2A_1 \overset{L_{20}}{\rightleftharpoons} A_2 \tag{16}$$

$$2A_2 \overset{L_{40}^{x}}{\rightleftharpoons} A_4 \tag{17}$$

$$L_2 = \frac{[A_2]}{[A_1]^2} \tag{18}$$

$$L_{40}^{x} = \frac{[A_4]}{[A_2]^2} \tag{19}$$

$$L_{20}^{2} L_{40}^{x} = L_{40} = \frac{[A_4]}{[A_1]^4} \tag{20}$$

Figure 9A−D shows the species fractions for monomers, dimers, and tetramers from simulations with $L_{20} = 1 \times 10^2$, 1×10^3, 1×10^4, 1×10^5 M^{-1} and L_{40}^{x} was calculated using eq 20 by maintaining $L_{40} = 1 \times 10^{15}$ M^{-3}, similar to the value we have determined from sedimentation equilibrium experiments. Figure 9A,B shows that for $L_{20} = 1 \times 10^2$ or 1×10^3 M^{-1}, respectively, the population of dimers is very small compared to the population of monomers and tetramers. Similarly, when $L_{20} = 1 \times 10^4$ M^{-1}, Figure 9C, the dimeric state is only slightly populated. Finally, only when $L_{20} = 1 \times 10^4$ M^{-1}, Figure 9D, or greater is the dimeric state significantly populated. These simulations of the species fractions suggest that sedimentation equilibrium experiments performed on a self-associating system that forms monomers, dimers, and tetramers with $L_{20} < 1 \times 10^4$ M^{-1} can be described by a monomer−tetramer equilibrium with no apparent dimer intermediates. This is similar to what we have observed experimentally. That is, when we forced our sedimentation equilibrium data to fit to a monomer−dimer−tetramer model, the rmsd value began to get worse when L_{20} exceeded 1×10^4 M^{-1}.

We have simulated mock sedimentation equilibrium data to test the possibility that ClpA could exist in a monomer−dimer−tetramer equilibrium at 25 °C but because the dimeric intermediate is not significantly populated the data can be described by a monomer−tetramer equilibrium and no information is present on the dimeric intermediate. We have simulated mock sedimentation equilibrium data using a monomer−dimer−tetramer model with the same equilibrium constants used to generate the species fractions shown in Figure 9A−D. To these data we introduced Gaussian distributed error of ~2%, as previously described (*42*). These "noisy" simulated data were then subjected to NLLS fitting with a monomer-*n*-mer model as described for the experimental data (see Materials and Methods). When simulated data are generated from a monomer−dimer−tetramer model with L_{20} between 1×10^2 and 1×10^4 M^{-1}, as in Figure 9A−C, and L_{40}^{x} constrained by the value of L_{20} and $L_{40} = 1 \times 10^{15}$ M^{-3} and subjected to global NLLS fitting, the data are best described by a monomer−tetramer model. That is to say, because the population of dimers is so low relative to monomers and tetramers, information on their presence is not apparent in the sedimentation equilibrium boundaries. In contrast, when sedimentation equilibrium boundaries are generated with $L_{20} = 1 \times 10^5$ M^{-1}, $L_{40}^{x} = 1 \times 10^5$ M^{-1}, and $L_{40} = 1 \times 10^{15}$ M^{-3}, as in Figure 9D, the data can be described by a monomer−trimer model however fits best to a monomer−dimer−tetramer model. These simulations suggest that if there are significantly populated dimers and tetramers and the data are analyzed with a two-species model then an apparent trimer appears, that is, an average size of a trimer from a dimer and tetramer, which we do not observe experimentally.

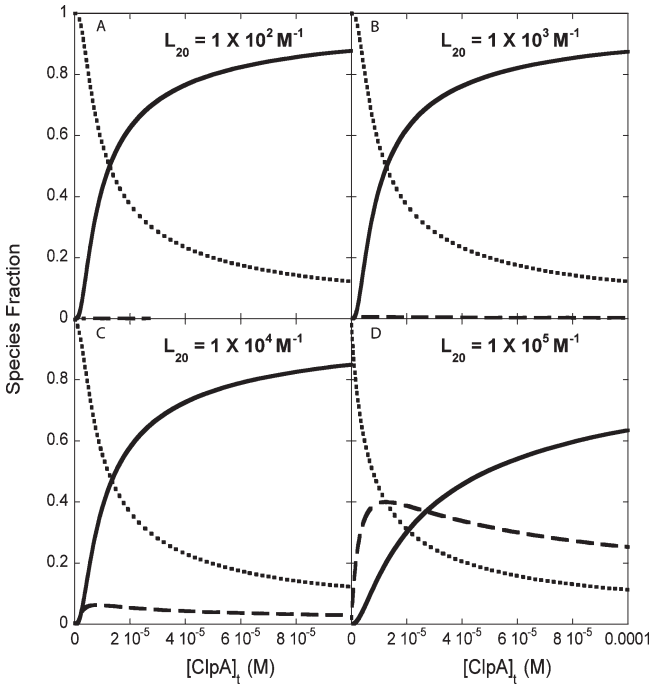

FIGURE 9: Monomer−dimer−tetramer species fraction simulations. (A−D) Individual simulations of monomer, dimer, and tetramer species fraction as a function of [ClpA] and L_{20} values of 1×10^2 M^{-1}, 1×10^3 M^{-1}, 1×10^4 M^{-1}, and 1×10^5 M^{-1} with a constrained overall equilibrium constant of 1×10^{15} M^{-3} . Monomer species fraction is plotted with a dotted line, dimer with a dashed line, and tetramer with a solid line. At low values of L_{20}, the species fraction of dimer is minute.

Our experimental data, presented above, is best described by a monomer−tetramer model. However, based on the above simulations and the NLLS analysis to various models we cannot rule out the possibility of a dimeric intermediate that is not significantly populated at 25 °C. That is to say, if dimers exist experimentally, these simulations allow us to place an upper limit on the equilibrium constant for dimer formation of $L_{20} < 1 \times 10^4$ M^{-1}. These results suggest that tetramer formation is highly cooperative at 25 °C. That is, if dimers are formed then the affinity for two dimers associating is much higher than for two monomers and thus there is no significantly populated dimeric intermediate.

It is widely accepted that ClpA resides in a monomer−dimer equilibrium in the absence of nucleoside triphosphate. However, this conclusion is based on a single sedimentation equilibrium experiment performed at 4 °C with two loading concentrations

(~2.4 and 6 μM monomer) and a single velocity (7000 rpm) (*19*). As such, the apparent discrepancy between our observation of a monomer−tetramer equilibrium at 25 °C versus the previously reported monomer−dimer equilibrium at 4 °C is likely due to the differences in temperature. Indeed, the monomer−dimer equilibrium constant and the dimer−tetramer equilibrium constant will depend on temperature. As such, it is entirely plausible that these two equilibrium constants will depend on temperature in such a way that one will observe only monomers and dimers at 4 °C but observe monomers and tetramers at 25 °C. Experiments to examine this possibility are underway. Currently, experiments performed at 4 °C are consistent with a monomer−dimer−tetramer model (P. Keith Veronese, manuscript in preparation).

Nucleotide Driven Hexamer Formation of ClpA. It has been previously established that ClpA requires nucleoside triphosphate and $MgCl_2$ to assemble into an oligomeric form capable of associating with the ClpP protease (*16*); however, the mechanism of this assembly process is not well understood. Kress and co-workers concluded that ClpA forms tetramers in the presence of ATPγS and the absence of Mg^{2+} at 25 °C using gel-filtration chromatography and stopped-flow static light scattering measurements (*23*). These authors concluded that the tetrameric intermediate they observed was a transient intermediate on the pathway to hexamer formation. Despite their experiments being performed at 25 °C, using the previously reported monomer−dimer equilibrium for ClpA determined at 4 °C, they propose a model for nucleotide driven hexamer formation. In their model ClpA is assumed to reside in a monomer−dimer equilibrium at 25 °C and upon addition of nucleoside triphosphate the dimers form tetramers and the tetramer associates with another dimer to form hexameric ClpA. Therefore, they conclude that the tetrameric state is a transient intermediate on the pathway to nucleotide-driven hexamer formation. Here, we report results showing that ClpA forms tetramers in the presence and absence of Mg^{2+} at 25 °C and thus the tetrameric intermediate observed by Kress and co-workers at 25 °C exists at thermodynamic equilibrium and is not simply a transient intermediate on the pathway to hexamer formation.

ClpA is a complex allosteric machine that both self-assembles and requires nucleoside triphosphate binding in order to assemble into a form capable of recognizing and binding target peptide sequences displayed by protein substrates and/or associate with the protease, ClpP. In order to quantitatively measure the binding affinity for ClpA binding different protein target sequences, and thereby address thermodynamic specificity, one must first obtain a quantitative description of nucleotide-driven hexamer formation. This is because any model describing binding to peptide sequences will be thermodynamically linked to both nucleotide binding and assembly. Therefore, in order to quantitatively examine the nucleotide-driven hexamer formation a detailed model of the self-association process in the absence of nucleotide is required. As it cannot be assumed that one model will persist at all temperatures and solution conditions such a detailed model must include an examination of the dependence of the self-association process on temperature and solution condition variables. As a consequence, we present here, the first step in such an examination and, underway, is a complete examination of the temperature dependence of self-association. Moreover, we have shown that ClpA is amenable to examination using these approaches.

ACKNOWLEDGMENT

We thank Dr. Karl Maluf for discussion throughout this research and his comments on the manuscript. We also thank Justin Miller and Dr. Rajendar Burki for their comments on the manuscript. In addition, we thank Dr. Peter Prevelige and the Department of Microbiology for the use of the Beckman XL-A Analytical Ultracentrifuge.

REFERENCES

1. Wickner, S., Maurizi, M. R., and Gottesman, S. (1999) Posttranslational quality control: folding, refolding, and degrading proteins. *Science 286*, 1888–1893.
2. Gottesman, S. (1996) Proteases and their targets in *Escherichia coli*. *Annu. Rev. Genet. 30*, 465–506.
3. Goldberg, A. L., and St. John, A. C. (1976) Intracellular protein degradation in mammalian and bacterial cells: Part 2. *Annu. Rev. Biochem. 45*, 747–803.
4. Sauer, R. T., Bolon, D. N., Burton, B. M., Burton, R. E., Flynn, J. M., Grant, R. A., Hersch, G. L., Joshi, S. A., Kenniston, J. A., Levchenko, I., Neher, S. B., Oakes, E. S., Siddiqui, S. M., Wah, D. A., and Baker, T. A. (2004) Sculpting the proteome with AAA(+) proteases and disassembly machines. *Cell 119*, 9–18.
5. Hwang, B. J., Woo, K. M., Goldberg, A. L., and Chung, C. H. (1988) Protease Ti, a new ATP-dependent protease in *Escherichia coli*, contains protein-activated ATPase and proteolytic functions in distinct subunits. *J. Biol. Chem. 263*, 8727–8734.
6. Katayama, Y., Gottesman, S., Pumphrey, J., Rudikoff, S., Clark, W. P., and Maurizi, M. R. (1988) The two-component, ATP-dependent Clp protease of *Escherichia coli*. Purification, cloning, and mutational analysis of the ATP-binding component. *J. Biol. Chem. 263*, 15226–15236.
7. Reid, B. G., Fenton, W. A., Horwich, A. L., and Weber-Ban, E. U. (2001) ClpA mediates directional translocation of substrate proteins into the ClpP protease. *Proc. Natl. Acad. Sci. U. S. A. 98*, 3768–3772.
8. Eytan, E., Ganoth, D., Armon, T., and Hershko, A. (1989) ATP-dependent incorporation of 20S protease into the 26S complex that degrades proteins conjugated to ubiquitin. *Proc. Natl. Acad. Sci. U. S. A. 86*, 7751–7755.
9. Hough, R., Pratt, G., and Rechsteiner, M. (1987) Purification of two high molecular weight proteases from rabbit reticulocyte lysate. *J. Biol. Chem. 262*, 8303–8313.
10. Dougan, D. A., Mogk, A., Zeth, K., Turgay, K., and Bukau, B. (2002) AAA+ proteins and substrate recognition, it all depends on their partner in crime. *FEBS Lett. 529*, 6–10.
11. Herman, C., Prakash, S., Lu, C. Z., Matouschek, A., and Gross, C. A. (2003) Lack of a robust unfoldase activity confers a unique level of substrate specificity to the universal AAA protease FtsH. *Mol. Cell 11*, 659–669.
12. Neuwald, A. F., Aravind, L., Spouge, J. L., and Koonin, E. V. (1999) AAA+: A class of chaperone-like ATPases associated with the assembly, operation, and disassembly of protein complexes. *Genome Res. 9*, 27–43.
13. Tucker, P. A., and Sallai, L. (2007) The AAA+ superfamily-a myriad of motions. *Curr. Opin. Struct. Biol. 17*, 641–652.
14. Walker, J. E., Saraste, M., Runswick, M. J., and Gay, N. J. (1982) Distantly related sequences in the alpha- and beta-subunits of ATP synthase, myosin, kinases and other ATP-requiring enzymes and a common nucleotide binding fold. *EMBO J. 1*, 945–951.
15. Gottesman, S., Squires, C., Pichersky, E., Carrington, M., Hobbs, M., Mattick, J. S., Dalrymple, B., Kuramitsu, H., Shiroza, T., and Foster, T.; et al. (1990) Conservation of the regulatory subunit for the Clp ATP-dependent protease in prokaryotes and eukaryotes. *Proc. Natl. Acad. Sci. U. S. A. 87*, 3513–3517.
16. Maurizi, M. R. (1992) Proteases and protein degradation in *Escherichia coli*. *Experientia 48*, 178–201.
17. Singh, S. K., and Maurizi, M. R. (1994) Mutational analysis demonstrates different functional roles for the two ATP-binding sites in ClpAP protease from *Escherichia coli*. *J. Biol. Chem. 269*, 29537–29545.
18. Kessel, M., Maurizi, M. R., Kim, B., Kocsis, E., Trus, B. L., Singh, S. K., and Steven, A. C. (1995) Homology in structural organization between *E. coli* ClpAP protease and the eukaryotic 26 S proteasome. *J. Mol. Biol. 250*, 587–594.
19. Maurizi, M. R., Singh, S. K., Thompson, M. W., Kessel, M., and Ginsburg, A. (1998) Molecular properties of ClpAP protease of

Escherichia coli: ATP-dependent association of ClpA and ClpP. *Biochemistry 37*, 7778–7786.
20. Guo, F., Maurizi, M. R., Esser, L., and Xia, D. (2002) Crystal structure of ClpA, an Hsp100 chaperone and regulator of ClpAP protease. *J. Biol. Chem. 277*, 46743–46752.
21. Guo, F., Esser, L., Singh, S. K., Maurizi, M. R., and Xia, D. (2002) Crystal structure of the heterodimeric complex of the adaptor, ClpS, with the N-domain of the AAA+ chaperone, ClpA. *J. Biol. Chem. 277*, 46753–46762.
22. Gottesman, S., Roche, E., Zhou, Y., and Sauer, R. T. (1998) The ClpXP and ClpAP proteases degrade proteins with carboxy-terminal peptide tails added by the SsrA-tagging system. *Genes Dev. 12*, 1338–1347.
23. Kress, W., Mutschler, H., and Weber-Ban, E. (2007) Assembly pathway of an AAA+ protein: tracking ClpA and ClpAP complex formation in real time. *Biochemistry 46*, 6183–6193.
24. Lohman, T. M., Chao, K., Green, J. M., Sage, S., and Runyon, G. T. (1989) Large-scale purification and characterization of the *Escherichia coli* rep gene product. *J. Biol. Chem. 264*, 10139–10147.
25. Schuck, P. (1998) Sedimentation analysis of noninteracting and self-associating solutes using numerical solutions to the Lamm equation. *Biophys. J. 75*, 1503–1512.
26. Schuck, P., and Rossmanith, P. (2000) Determination of the sedimentation coefficient distribution by least-squares boundary modeling. *Biopolymers 54*, 328–341.
27. Schuck, P. (2003) On the analysis of protein self-association by sedimentation velocity analytical ultracentrifugation. *Anal. Biochem. 320*, 104–124.
28. Dam, J., and Schuck, P. (2005) Sedimentation velocity analysis of heterogeneous protein-protein interactions: sedimentation coefficient distributions c(s) and asymptotic boundary profiles from Gilbert-Jenkins theory. *Biophys. J. 89*, 651–666.
29. Cole, J. L. (2004) Analysis of heterogeneous interactions. *Methods Enzymol. 384*, 212–232.
30. Taylor, J. R. (1997) An Introduction to Error Analysis: The Study of Uncertainties in Physical Measurements , University Science Books, Sausalito, CA.
31. Correia, J. J. (2000) Analysis of weight average sedimentation velocity data. *Methods Enzymol. 321*, 81–100.
32. Berne, B. J., Pecora, R. (2000) Dynamic Light Scattering: with Applications to Chemistry, Biology, and Physics , Dover Publications, Mineola, N.Y.
33. Dennis, E. K. (1972) Analysis of macromolecular polydispersity in intensity correlation spectroscopy: the method of cumulants. *J. Chem. Phys. 57*, 4814–4820.
34. Bujalowski, W., Klonowska, M. M., and Jezewska, M. J. (1994) Oligomeric structure of *Escherichia coli* primary replicative helicase DnaB protein. *J. Biol. Chem. 269*, 31350–31358.
35. Tanford, C. 1961. Physical Chemistry of Macromolecules, Wiley, New York.
36. Maluf, N. K., and Lohman, T. M. (2003) Self-association equilibria of *Escherichia coli* UvrD helicase studied by analytical ultracentrifugation. *J. Mol. Biol. 325*, 889–912.
37. Kuntz, I. D. (1971) Hydration of macromolecules. IV. Polypeptide conformation in frozen solutions. *J. Am. Chem. Soc. 93*, 516–518.
38. Lin, T. H., Quinn, T., Walsh, M., Grandgenett, D., and Lee, J. C. (1991) Avian myeloblastosis virus reverse transcriptase. Effect of glycerol on its hydrodynamic properties. *J. Biol. Chem. 266*, 1635–1640.
39. Correia, J. J., and Stafford, W. F. (2009) Extracting equilibrium constants from kinetically limited reacting systems. *Methods Enzymol. 455*, 419–446.
40. Cole, J. L., Lary, J. W., P. M. T, and Laue, T. M. (2008) Analytical ultracentrifugation: sedimentation velocity and sedimentation equilibrium. *Methods Cell Biol. 84*, 143–179.
41. Garcia de la Torre, J. G., and Bloomfield, V. A. (1981) Hydrodynamic properties of complex, rigid, biological macromolecules: theory and applications. *Q. Rev. Biophys. 14*, 81–139.
42. Lucius, A. L., Vindigni, A., Gregorian, R., Ali, J. A., Taylor, A. F., Smith, G. R., and Lohman, T. M. (2002) DNA unwinding step-size of *E. coli* RecBCD helicase determined from single turnover chemical quenched-flow kinetic studies. *J. Mol. Biol. 324*, 409–428.